Bone & Joint Research

Supplementary Material

10.1302/2046-3758.135.BJR-2023-0320.R1

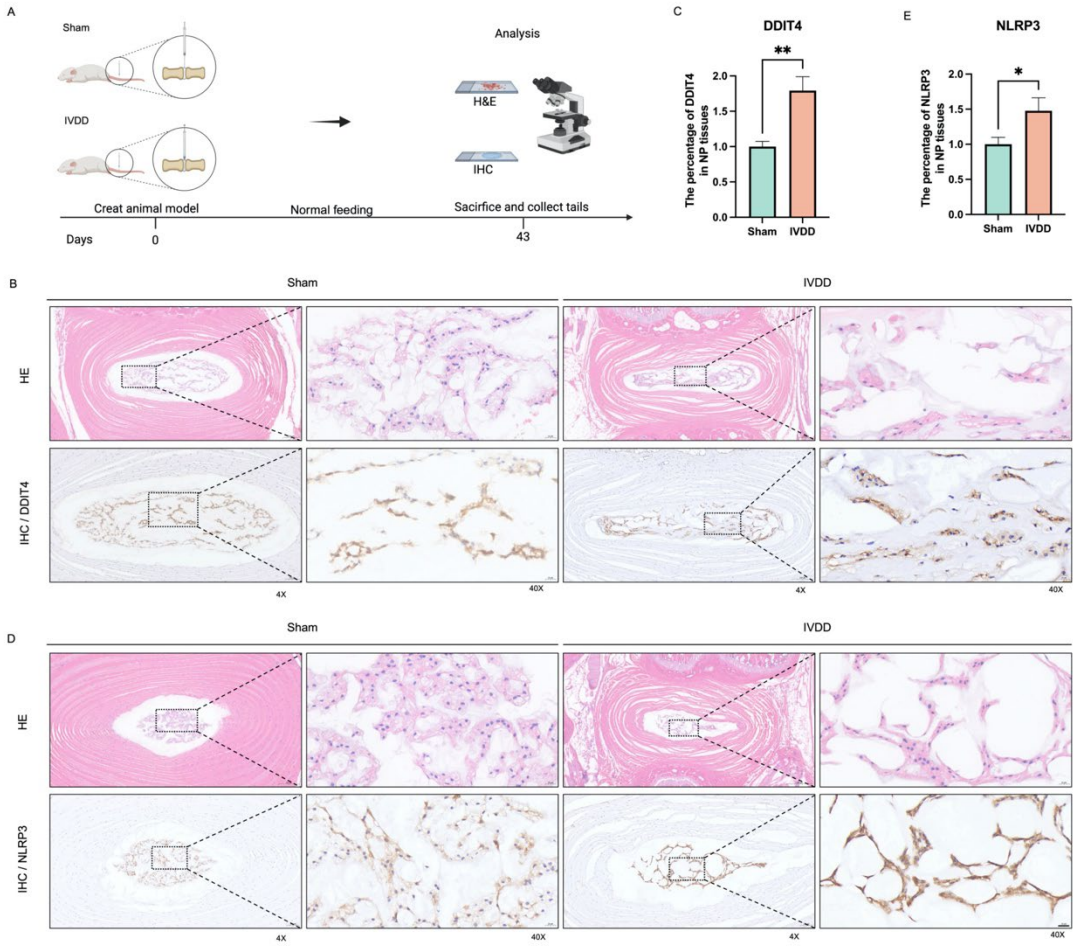

Fig a. Intervertebral disc degeneration (IVDD) rat modeling procedure and histological staining. a)The process of establishing IVDD model by acupuncture in rat tail. b) to e) Haematoxylin and eosin (H&E) staining with different degrees of aggregation, IHC staining, and quantitative analysis of DDIT4 and NLRP3 in the sham and acupuncture-induced IVDD groups (n = 6). Scale bars in overall view: 200 μm; scale bars in local view: 20 μm. Data are expressed as the mean and standard deviation (*p < 0.05; **p < 0.01).

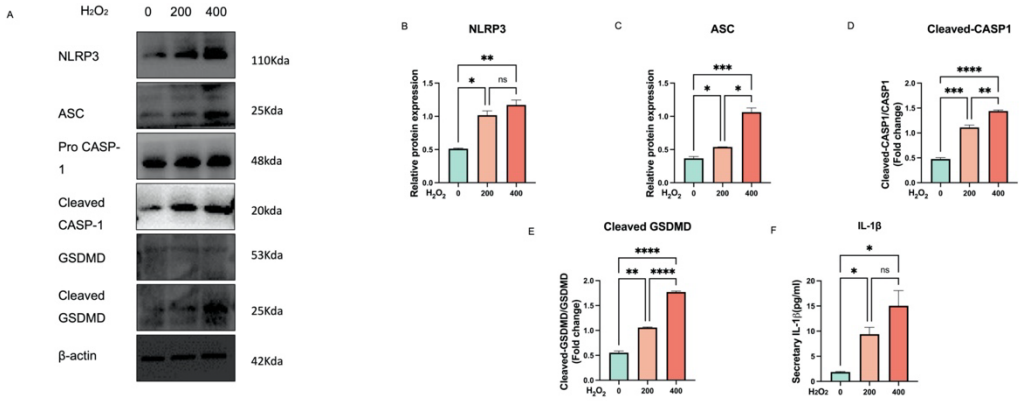

Fig b. After interfering with nucleus pulposus cells (NPCs) with different concentrations of hydrogen peroxide, the expressions of NLRP3, ASC, cleaved CASP1, cleaved-GSDMD, and interleukin 1 beta (IL-1β) were detected. a) Western blotting of NLRP3, ASC, pro-CASP-1, cleaved CASP-1, GSDMD, and cleaved GSDMD in hydrogen peroxide-treated NPCs. b) to c) Western blotting quantitative analysis of NLRP3 and ASC in hydrogen peroxide-treated NPCs. d) Ratio of cleaved CASP-1 to pro-CASP-1 in hydrogen peroxide-treated NPCs and control NPCs. e) Ratio of cleaved GSDMD to GSDMD in hydrogen peroxide-treated NPCs. f) Quantitative analysis of IL-1β in cell culture supernatants after hydrogen peroxide treatment. ns, not significant. *p < 0.05; **p < 0.01; ***p < 0.001; ****p < 0.0001.

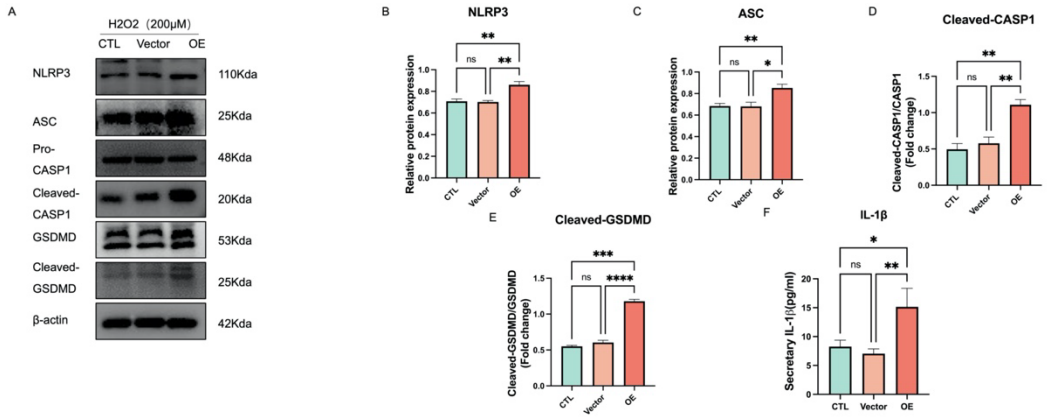

Fig c. The expression of NLRP3, ASC, cleaved CASP1, cleaved-GSDMD, and interleukin 1 beta (IL-1β) after DNA-damage-inducible transcript 4 (DDIT4) overexpression was detected. a) Representative images of western blotting of NLRP3, ASC, pro-CASP-1, cleaved CASP-1, GSDMD, and cleaved GSDMD after overexpression. b) to c) Western blot quantitative analysis of NLRP3 and ASC after overexpression of DDIT4. d) Ratio of cleaved CASP-1 to pro-CASP-1 after hydrogen peroxide treatment in the control, vector, and overexpression groups.

e) Ratio of cleaved GSDMD to GSDMD in NPCs treated with hydrogen peroxide in the control, vector, and overexpression groups. f) Quantitative analysis of interleukin 1 beta (IL-1β) in the culture supernatant of NPCs treated with hydrogen peroxide in the control, vector, and overexpression groups. Data are expressed as the mean and standard deviation of at least three independent experiments. Two-way analysis of variance was used for statistical analysis. ns, not significant. *p < 0.05; **p < 0.01; ***p < 0.001; ****p < 0.0001.

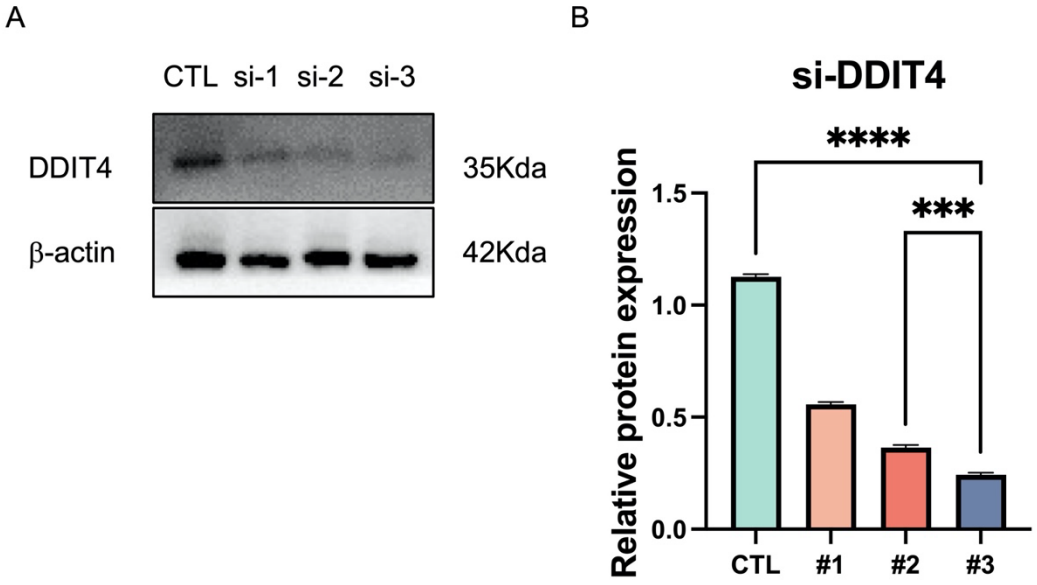

Fig d. Western blot detection of DNA-damage-inducible transcript 4 (DDIT4) expression after co-intervention with three types of small interfering RNA (siRNA) in nucleus pulposus cells (NPCs). a) and b) Representative images of western blotting and quantification of DDIT4 in NPCs treated with hydrogen peroxide after knockdown of DDIT4 by siRNAs numbered 1, 2, and 3 compared to control group.

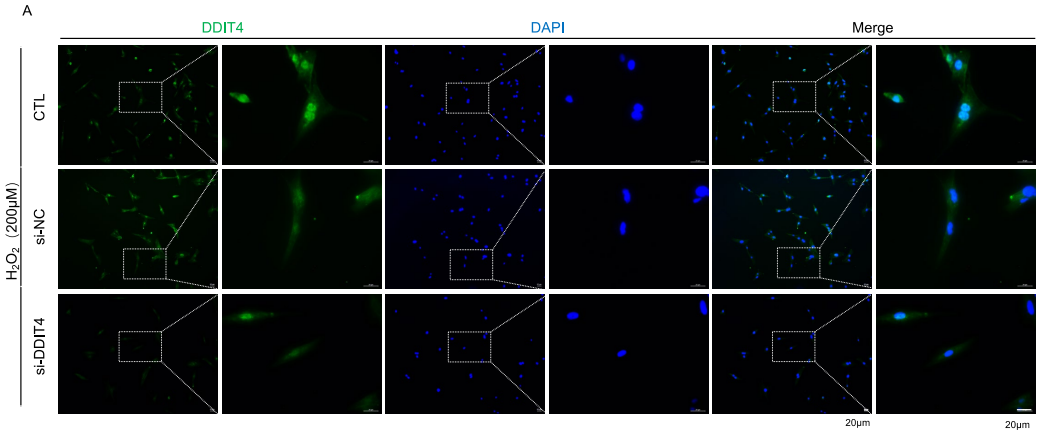

Fig e. Immunofluorescence was used to detect DNA-damage-inducible transcript 4 (DDIT4) expression in the nucleus pulposus cells of the control, negative control and small interfering DDIT4 (siDDIT4) groups following hydrogen peroxide intervention. Immunofluorescence images of different polymerization degrees of DDIT4 after siRNA knockdown and hydrogen peroxide treatment; scale bars: 20 μm.

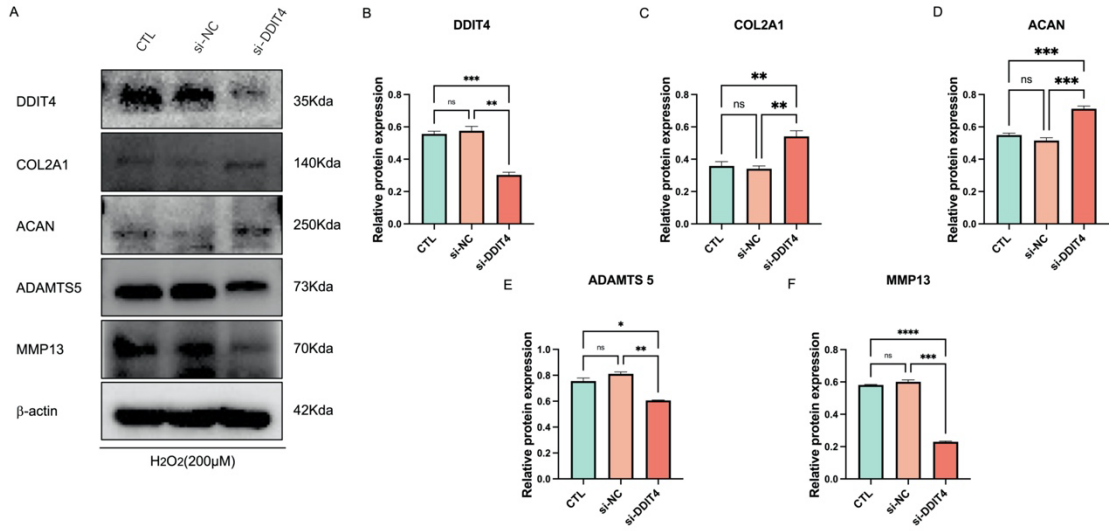

Fig f. The western blot analysis revealed the expression of DNA-damage-inducible transcript 4 (DDIT4), COL2A1, ACAN, matrix metalloproteinase 13 (MMP13), and ADAMTS5 subsequent to DDIT4 knockdown. a) Representative images of western blotting of DDIT4, COL2A1, ACAN, ADAMTS5, and MMP13 after hydrogen peroxide treatment in the control, negative control, and knockdown groups. b) to f) Quantitative analysis of DDIT4, COL2A1, ACAN, ADAMTS5, and MMP13 after hydrogen peroxide treatment in the control,

negative control, and knockdown groups. Data are expressed as the mean and standard deviation of at least three independent experiments. Two-way analysis of variance was used for statistical analysis. ns, not significant. *p < 0.05; **p < 0.01; ***p < 0.001; ****p < 0.0001.

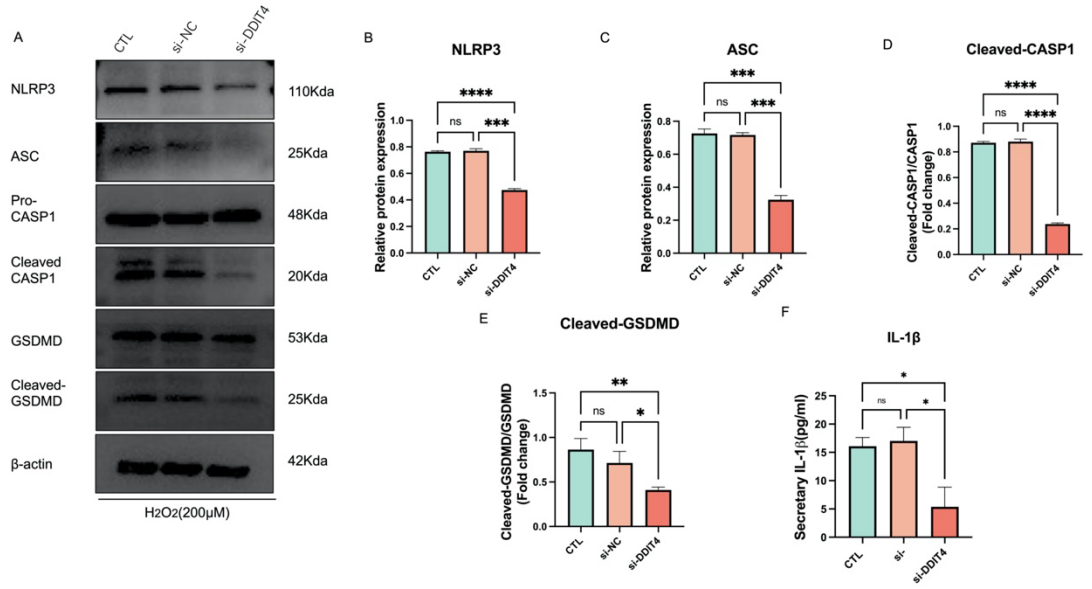

Fig h. The expression of NLRP3, ASC, cleaved CASP1, cleaved-GSDMD, and interleukin 1 beta (IL-1β) after DNA-damage-inducible transcript 4 (DDIT4) knockdown was detected. a) Representative images of western blotting of NLRP3, ASC, cleaved-CASP1, and cleaved-GSDMD after hydrogen peroxide treatment in the control, negative control, and knockdown groups. b) and c) Quantitative analysis of NLRP3 and ASC after knockdown of DDIT4. d) Ratio of cleaved CASP-1 to pro-CASP-1 after knockdown of DDIT4. e) Ratio of cleaved GSDMD to GSDMD after knockdown of DDIT4. f) Quantitative analysis of IL-1β in the culture supernatant of nucleus pulposus cells after knockdown of DDIT4. Data are expressed as the mean and standard deviation of at least three independent experiments. Two-way analysis of variance was used for statistical analysis. ns, not significant. *p < 0.05; **p < 0.01; ***p < 0.001; ****p < 0.0001.

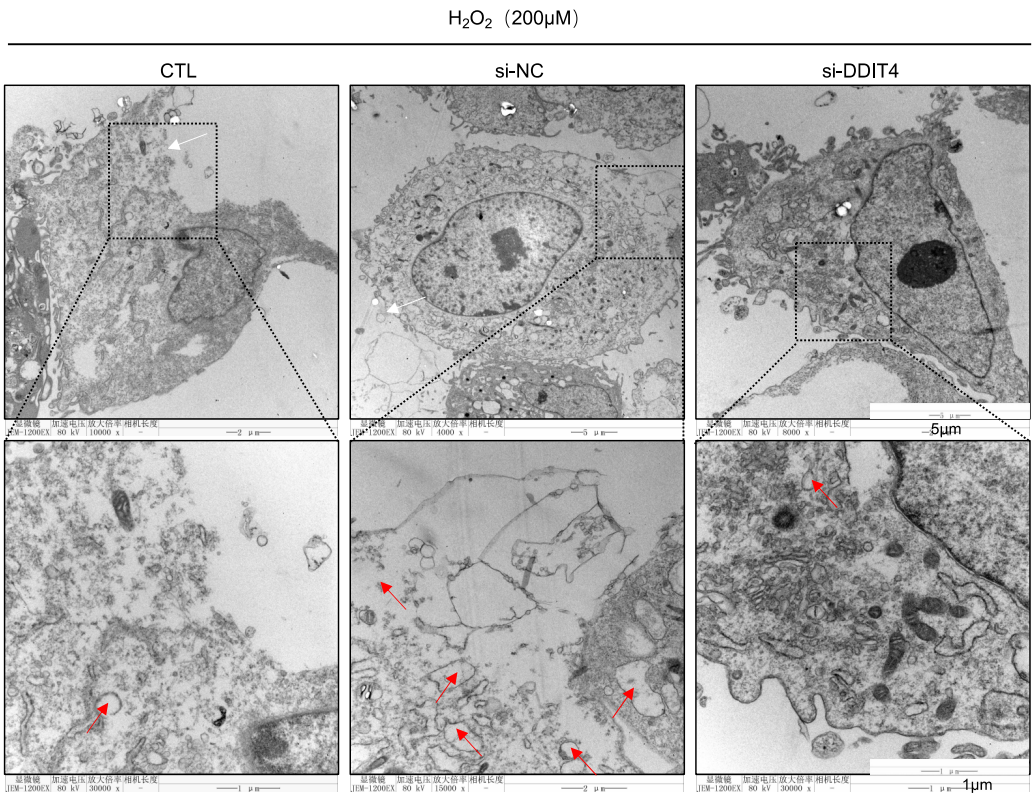

Fig i. Transmission electron microscopy was conducted to analyze the ultrastructure of nucleus pulposus cells (NPCs) subsequent to DNA-damage-inducible transcript 4 knockdown (DDIT4), such as cytoplasmic oedema, swelling of cell membrane, karyopyknosis, and organelle cavitation. White arrows show swelling of cell membrane; red arrows show organelle cavitation. Scale bars in overall view: 5 μm. Scale bars in local view: 1 μm.

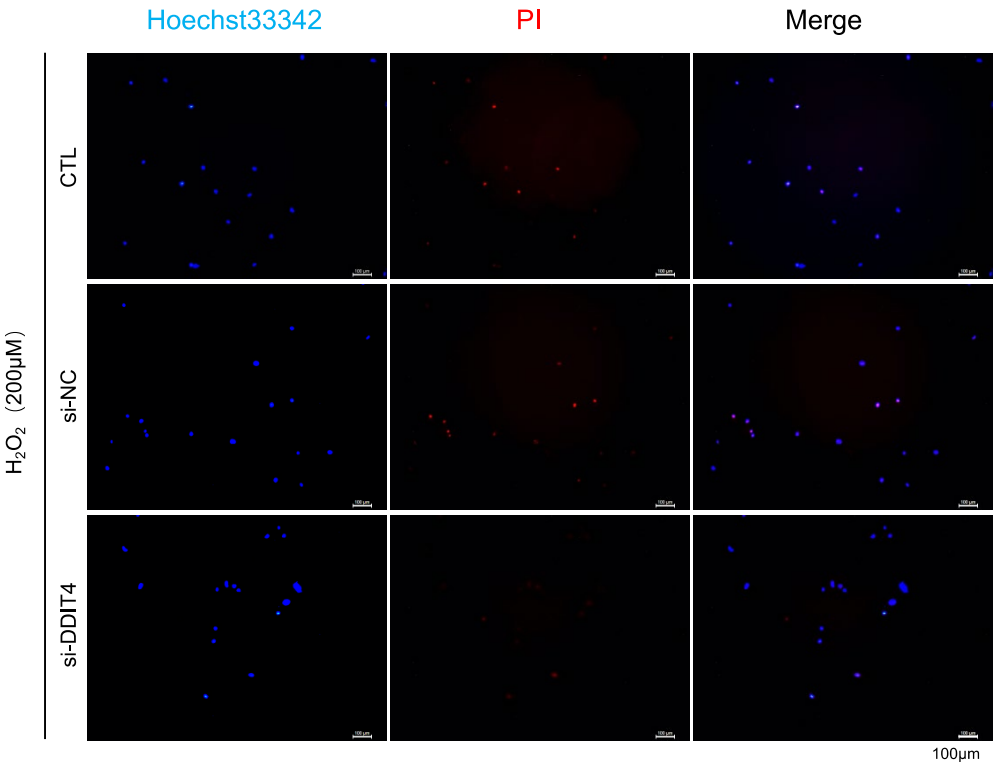

Fig j. Representative fluorescence images of Hoechst 33342/PI staining of nucleus pulposus cells after knockdown of DNA-damage-inducible transcript 4 knockdown (DDIT4). Scale bars, 100 μm.

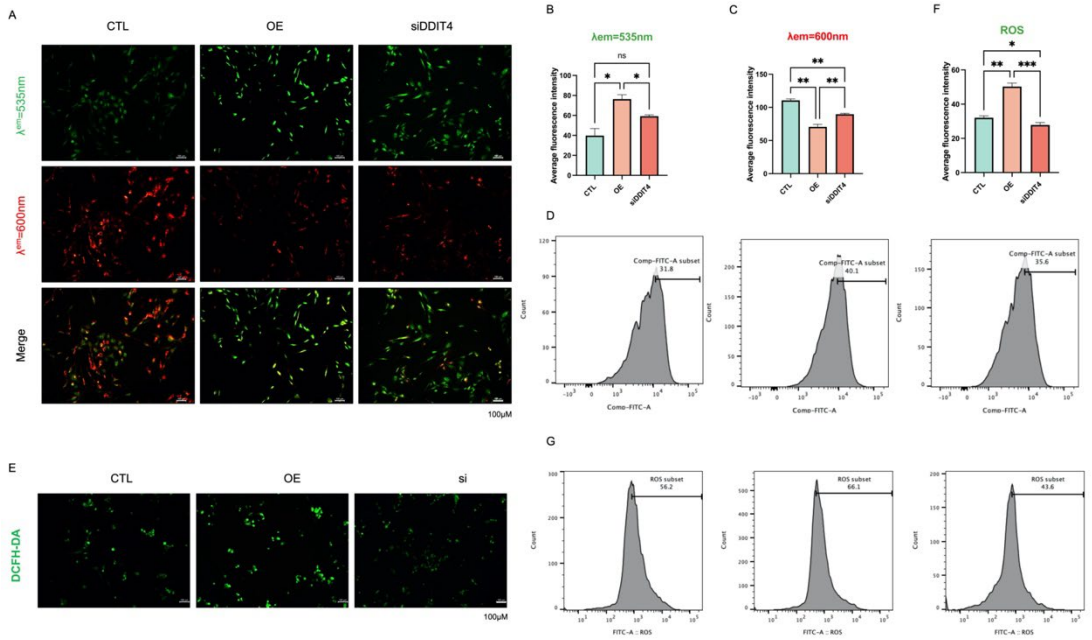

Fig k. DNA-damage-inducible transcript 4 (DDIT4) impairs mitochondrial function and promotes reactive oxygen species (ROS) generation nucleus pulposus cells (NPCs) in the control, overexpression, and knockdown groups were cultured for 24 hours. a) to c) JC-1 staining intensity under different excitation wavelengths, with quantitative analysis of fluorescence. The ratio of red-to-green fluorescence reflects changes in mitochondrial membrane potential in NPCs; scale bars: 20 μm. d) Flowcytometry with JC-1 staining was used to detect changes in the mitochondrial membrane potential of NPCs. e) ROS were detected in NPCs using the dichloro-dihydro-fluorescein diacetate (DCFH-DA) probe. Green fluorescence represents the level of ROS in the cells; scale bars: 20 μm. f) Quantitative analysis of ROS fluorescence intensity. g) Flowcytometry was performed using the DCFH-DA probe to detect ROS in NPCs. Data are expressed as the mean and standard deviation of at least three independent experiments. Two-way analysis of variance was used for statistical analysis (ns, no statistical significance; *$p < 0.05$; **$p < 0.01$; ***$p < 0.001$; ****$p < 0.0001$).

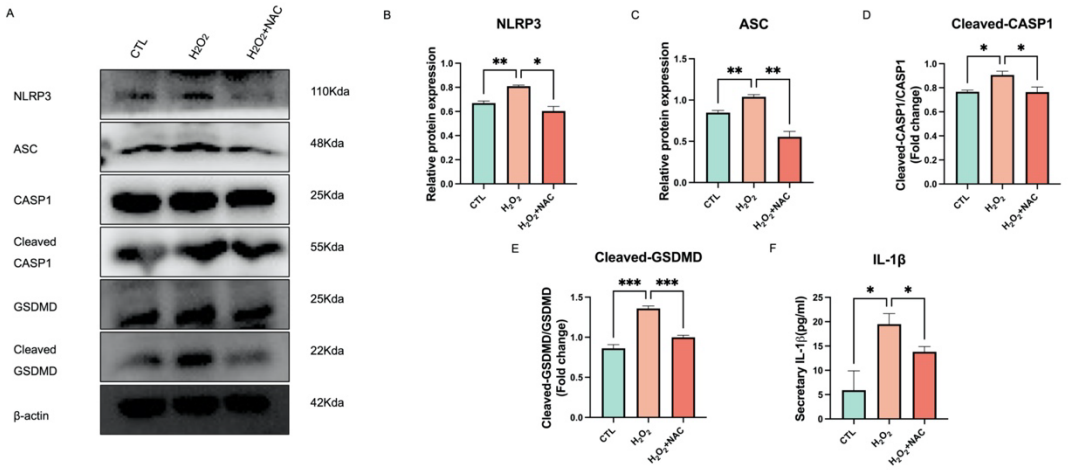

Fig I. DNA-damage-inducible transcript 4 (DDIT4) mediated pyroptosis of nucleus pulposus cells (NPCs) through the ROS–-NLRP3–-CASP1 axis. a) Representative images of western blotting of NLRP3, ASC, pro-CASP-1, cleaved CASP-1, GSDMD, and cleaved GSDMD in NPCs in the control, hydrogen peroxide treatment, and NAC treatment groups. b) and c) Quantification of NLRP3 and ASC protein levels in NPCs in the control, hydrogen peroxide treatment, and NAC treatment groups. d) Ratio of cleaved CASP-1 to native CASP-1 in NPCs in the control, hydrogen peroxide treatment, and NAC treatment groups. e) Ratio of cleaved GSDMD to original GSDMD in NPCs in the control, hydrogen peroxide treatment, and NAC treatment groups. f) Quantitative analysis of interleukin 1 beta (IL-1β) in the culture supernatants of NPCs in the control, hydrogen peroxide treatment, and NAC treatment groups. Data are expressed as the mean and standard deviation of at least three independent experiments. Independent-samples *t*-test and two-way analysis of variance were used for statistical analysis (ns, no statistical significance; *p < 0.05; **p < 0.01; ***p < 0.001).

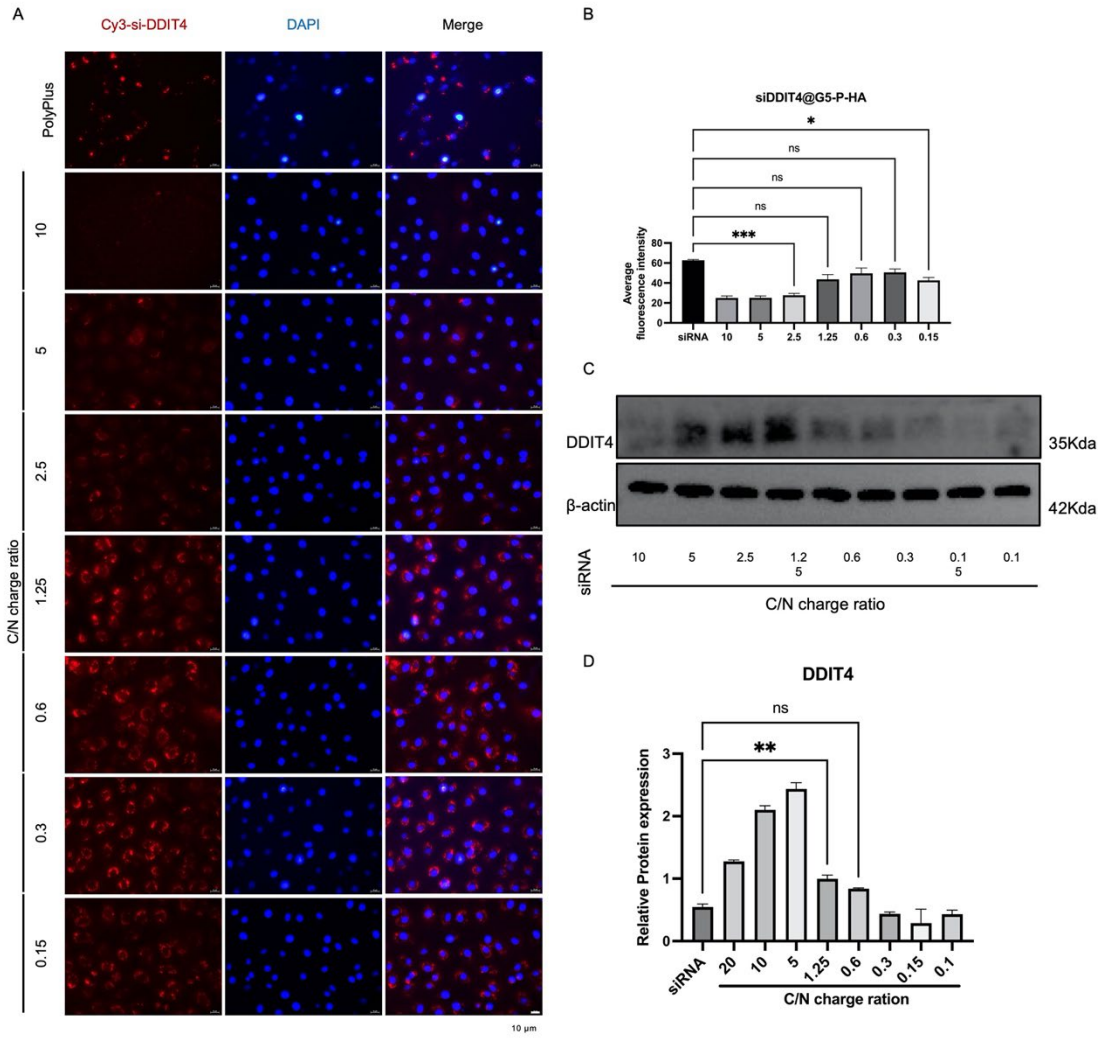

Fig m. Assessment of siDDIT4@G5-P-HA hydrogels' cellular uptake and silencing efficiency. a) Representative fluorescence images of intracellular uptake of siRNAs in the cy3-siDDIT4@Polyplus and cy3-siDDIT4@G5-P-HA groups. Red represents cy3-labelled siDDIT4, and blue represents DAPI-labelled nuclei; scale bars: 10 μm. b) Quantitative analysis of positive cells in fluorescence images. c) and d) Representative western blotting and quantitative analysis of DDIT4 expression in NPCs treated with siDDIT4@G5-P-HA. Data are expressed as the mean and standard deviation of at least three independent experiments. Two-way analysis of variance and independent-samples *t*-test were used for statistical analysis (ns, no statistical significance; *p < 0.05; **p < 0.01; ***p < 0.001).

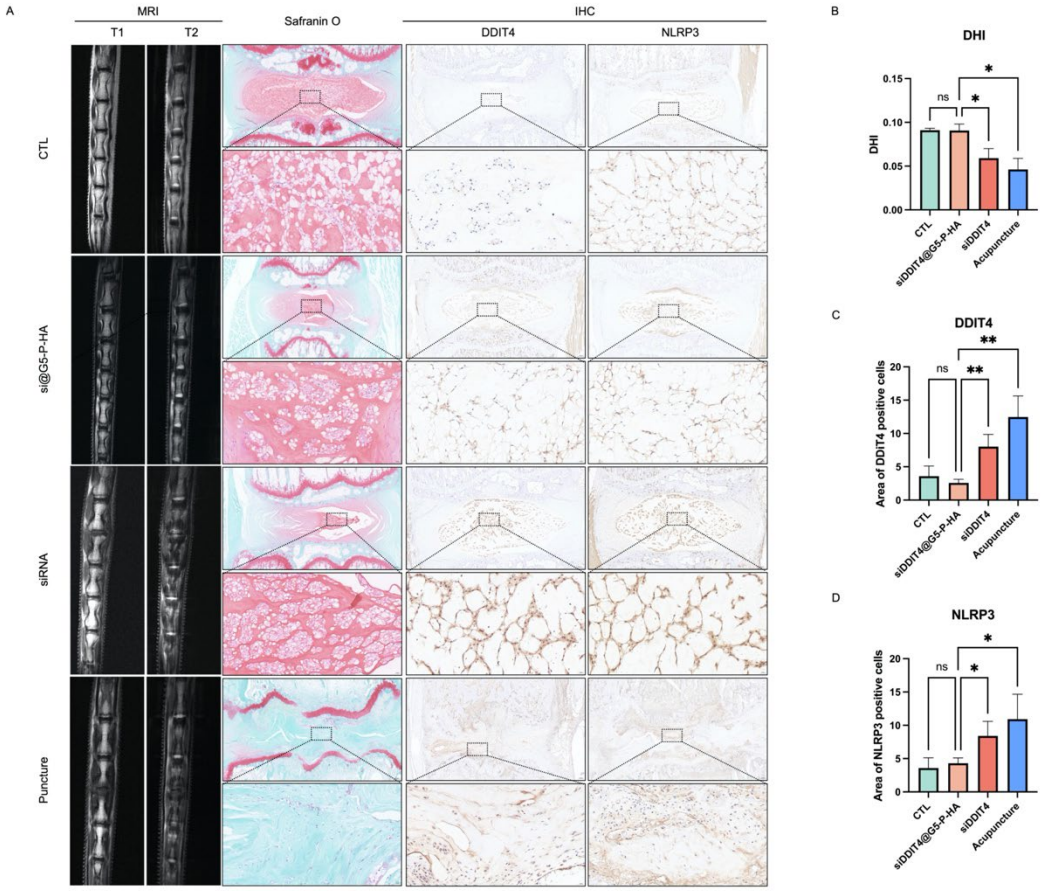

Fig n. siDDIT4@G5-P-HA delays the progression of intervertebral disc degeneration (IVDD) in rat models of acupuncture-induced IVDD. a) Representative images of MRI, safranin O staining, and immunohistochemical analysis of DDIT4 and NLRP3 in the control, siDDIT4@G5-P-HA, siDDIT4, and acupuncture groups. b) Quantitative analysis of DHI in the control, siDDIT4@G5-P-HA, siDDIT4, and acupuncture groups. c) Immunohistochemical analysis of DDIT4 in the control, siDDIT4@G5-P-HA, siDDIT4, and acupuncture groups. d) Immunohistochemical analysis of NLRP3 in the control, siDDIT4@G5-P-HA, siDDIT4, and acupuncture groups. Data are expressed as the mean and standard deviation. Two-way analysis of variance and independent-samples *t*-test were used for statistical analysis (ns, no statistical significance; *$p < 0.05$; **$p < 0.01$; ***$p < 0.001$).